Research Article | Vol. 30, No. 20 / 26 Sep 2022 / Optics Express 36644

Optics EXPRESS

Correcting the wavelength-induced phase deviation of Pancharatnam-Berry lenses

ZHENYI LUO,[1] JUNYU ZOU,[1] EN ZHAO,[2] YI RAO,[2] AND SHIN-TSON WU[1,*]

[1]College of Optics and Photonics, University of Central Florida, Orlando, Florida 32816, USA
[2]Goertek Electronics, 5451 Great America Parkway, Suite 301, Santa Clara, CA 95054, USA
[*]swu@creol.ucf.edu

Abstract: Liquid-crystal-based Pancharatnam-Berry optical elements are widely used in virtual reality and augmented reality. However, the mismatch between exposure wavelength and operating wavelength leads to an undesirable phase deviation to the lenses, which in turn causes severe aberration especially when the f-number is small. To overcome the mismatched wavelength problem and to obtain a nearly ideal lens phase profile, a new exposure method using two template lenses with different focal lengths is proposed and experimentally validated. Our results indicate that such a lens indeed exhibits a better imaging performance than that fabricated by traditional interference method.

1. Introduction

Unlike a refractive optical device that generates phase pattern using the optical pathlength difference, liquid-crystal (LC)-based Pancharatnam-Berry optical element (PBOE), which can be regarded as a patterned half-wave plate, produces desired phase profile by spatially varying the LC directors [1–7]. With the advantages of high diffraction efficiency (nearly 100%), polarization selectivity, ultrathin formfactor, and dynamic switching, PBOE has found promising applications in near-eye display systems [8–11].

The underlying operation principle of PBOEs can be described by following equation using Jones matrix representation:

$$J'_{\pm} = \frac{1}{\sqrt{2}} \begin{bmatrix} \cos 2\phi & \sin 2\phi \\ \sin 2\phi & -\cos 2\phi \end{bmatrix} \begin{bmatrix} 1 \\ \pm i \end{bmatrix} = \frac{1}{\sqrt{2}} \begin{bmatrix} 1 \\ \mp i \end{bmatrix} e^{\pm 2i\phi}, \tag{1}$$

where ϕ is the azimuthal angle of the LC directors. As Eq. (1) indicates, when a left- or right-handed circularly polarized light (LCP and RCP) passing through the optical elements, its polarization state is switched, and the output beam also carries an extra 2ϕ phase. Various distribution of ϕ can be achieved by a proper LC alignment method. Based on different phase distribution, many types of PBOEs have been demonstrated [12–15]. Among them, PB lenses have found potential applications in augmented reality (AR) and virtual reality (VR) headsets.

To obtain the desired LC distribution, several methods have been developed while surface alignment is the most established one for PBOE fabrication [16,17]. With the help of photo-alignment (PA) materials that are sensitive to the incident polarization, the desired phase pattern can be recorded using Mach-Zehnder Interferometer (MZI). However, the effective exposing wavelength is restricted by the absorption spectrum of the PA materials. For example, brilliant yellow (BY), a widely used PA material, shows an absorption peak at λ=432 nm [18], which means the exposure wavelength should be in the blue spectral region. The phase profile of a PB lens (PBL) with a focal length of f_0 is $2\pi\sqrt{r^2 + f_o^2}/\lambda_o$, where λ_o is the operating wavelength and r is the radius of the PBL. When designing and fabricating a PBL for a red wavelength, the mismatch between exposing and operating wavelengths will result in a phase deviation, which

#473679 https://doi.org/10.1364/OE.473679
Journal © 2022 Received 21 Aug 2022; revised 7 Sep 2022; accepted 7 Sep 2022; published 21 Sep 2022

Optics EXPRESS

equals to $2\pi\left(\sqrt{r^2+f_o^2}/\lambda_o - \sqrt{r^2+f_e^2}/\lambda_e\right)$, where f_e is the focal length of the template lens and λ_e is the exposing wavelength. The incurred phase difference would degrade the imaging quality and limit its applications for AR/VR displays. Freeform lenses offer potential solutions to this problem and provide desired phase profile for the exposure of PBLs [19]. However, the design and fabrication process of freeform lenses are challenging. Meanwhile, each designed freeform lens is only applicable for the exposure of PBL with a fixed focal length and operating wavelength. These drawbacks limit the application of freeform lenses in the fabrication process of PBLs and more convenient approaches are needed to solve the wavelength-induced phase deviation.

In this paper, a new method for fabricating PBLs is demonstrated to correct the wavelength-induced phase deviation. In traditional PBL fabrication methods, the phase profile of only one template lens is recorded by the PA material. Here, we employ two different template lenses in different arms of MZI and record their phase profile difference by the PA material, which enables a more accurate phase profile control of the PBL. The intensity distribution of the PBL is measured and compared with simulation results. Good agreement is obtained. Moreover, the imaging characteristics of PBLs are investigated using a Maxwellian display system and the performance improvement is quite noticeable.

2. Design and fabrication

In a VR system, due to the etendue conservation [10], a small f-number imaging lens helps to reduce the depth of the headset. The f-number of a lens is defined as f/D, where f is the focal length and D is the diameter of the entrance pupil. To achieve a compact and lightweight VR display, PBLs with a small f-number are favorable, if the above-mentioned phase deviation problem can be alleviated. To obtain the desired phase profile, let us consider the interference of RCP and LCP beams with different phase patterns. The interference can be expressed using Jones matrix representation as:

$$J = \begin{bmatrix} 1 \\ -i \end{bmatrix} e^{i\alpha} + \begin{bmatrix} 1 \\ i \end{bmatrix} e^{i\beta} = 2 \begin{bmatrix} \cos\frac{\alpha-\beta}{2} \\ \sin\frac{\alpha-\beta}{2} \end{bmatrix} e^{i\frac{\alpha+\beta}{2}}, \tag{2}$$

where α and β represent the phase pattern of RCP and LCP beams, respectively. As Eq. (2) indicates, the recorded phase pattern is the difference between RCP and LCP beams, which provides one more degree of freedom to manipulate the phase profile of PBOE, and $\phi = (\alpha - \beta)/2$ is the azimuthal angle of the LC director defined in Eq. (1). After spin-coating an LC layer, the phase can be recovered when a circularly polarized light traverses the device.

Based on the above analysis, we design two lenses PBL-1 and PBL-2 for comparison. For PBL-1, the phase profile of a 5.56-cm lens (at $\lambda = 457$ nm) is used in the MZI to obtain a focal length of 4 cm at $\lambda = 635$ nm. In this case, either α or β is equal to 0, depending on which arm the lens is placed. To achieve the same focal length for PBL-2, two template lenses with focal lengths (4.32 cm and 19.41 cm at $\lambda = 457$ nm) are employed. The procedures to find the focal lengths of these two lenses are briefly outlined as follows. We first enumerate the possible combinations of focal lengths in the 1.5-cm to 20-cm range for the PBL with 4-cm focal length. For each case with two different focal lengths, the phase ϕ_1 to be recorded is the difference between the phase profiles corresponding to the two focal lengths according to Eq. (2). Then, each ϕ_1 is compared to the ideal phase profile ϕ_2 of the desired lens. Then the phase difference $\Delta\phi = \phi_1 - \phi_2$ can be calculated. By analyzing the distribution of $\Delta\phi$ along radius, the combination with minimum variance can be obtained. Finally, the two focal lengths in this combination are the desired results. The phase profile of these two PBLs are compared with an ideal lens and their differences are plotted in Fig. 1(a). The phase deviation caused by the wavelength mismatch of PBL-1 increases dramatically as the lens radius (r) exceeds 5 mm. Meanwhile, for PBL-2, the difference of phase pattern is much smaller and remains in an acceptable range.

Optics EXPRESS

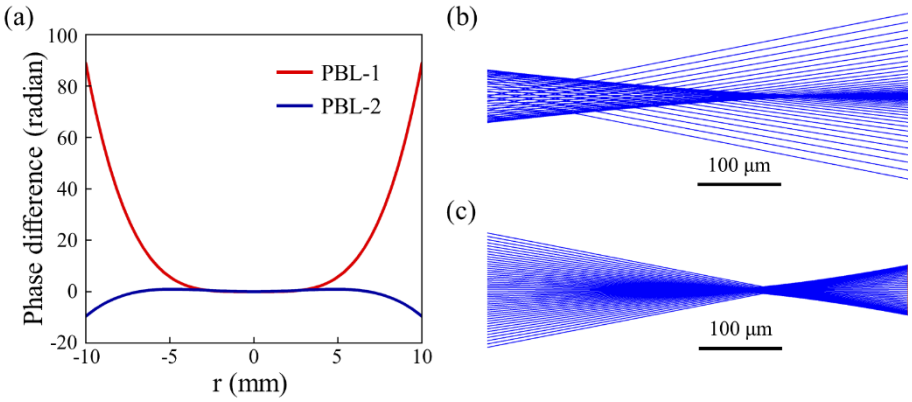

Fig. 1. (a) Simulated phase difference between PBL-1 and PBL-2 in comparison with an ideal lens (r = lens radius). Ray tracing around the focal point of (b) PBL-1 and (c) PBL-2.

In addition to calculate the phase profiles, raytracing is also employed to simulate the performances of the designed lenses. Considering the case when a collimated incident beam traverses through the designed lenses, the ray bundle around the focal point is illustrated in Fig. 1(b) and 1(c). The rays that passing through an ideal lens are expected to converge to a single spot. However, for PBL-1 exposed using one lens, the rays diffracted by different positions of the lens spreads out in a large range. Compared to PBL-1, the diffracted ray bundle of PBL-2 is focused to a much tighter spot because the phase difference between PBL-2 and the ideal lens is relatively small, as Fig. 1(a) depicts.

In experiment, the lens pattens were recorded using surface alignment method. Firstly, the PA material BY was dissolved in dimethyl-formamide and then spin-coated on a clean glass [20]. The material ratio and spin-coating speed are listed in Table 1. After spin coating, the PA layer was exposed using the setup depicted in Fig. 2. The 457-nm laser beam first passed through an objective lens, a spatial filter, and then a collimating lens. The beam was then split into two components by the first beam splitter (BS_1). The two linearly polarized beams were converted into RCP and LCP, respectively, using the quarter-wave plates (QWP_1 and QWP_2). Let us assume RCP passing through L_1 whose focal length is 19.41-cm and LCP passing through L_2 whose focal length is 4.32-cm. A second beam splitter BS_2 was used to combine the two phase-modified beams and merge the two optical paths together. To record the phase pattern precisely, the optical paths should be finetuned, and the centers of the two lens patterns overlapped with each other. After optimizing the setup, the PA layer was exposed to a laser output at 150 mW/cm^2 for about 2 min. With the designed phase patterns recorded, two LC layers (Table 1) were spin-coated on the PA layer to satisfy the half-wave condition at $\lambda = 635$ nm. Afterwards, the spin-coated substrate was exposed to UV light to stabilize the polymerization process. In contrast to PBL-2, PBL-1 was also fabricated using the MZI setup shown in Fig. 2 but only with a 5.56-cm lens at $\lambda = 457$ nm.

Table 1. Materials and coating speed for fabricating PBLs.

	Solute	Solvent	Solute: Solvent	Coating Speed
Alignment layer	Brilliant Yellow	Dimethyformamide	1:499	500 (5s) + 3000 (30s)
1st LC layer	RM257 (96.9%) Irgacure 651 (3%)	Tolune	1:3	2000 (30s)
2nd LC layer	Zonyl 8857A (0.1%)		1:5	2000 (30s)

Optics EXPRESS

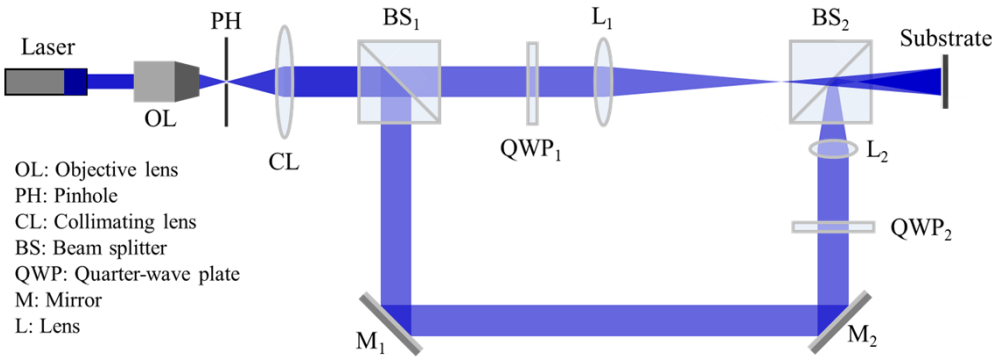

Fig. 2. Mach-Zehnder interferometer for fabricating PBL-2.

3. Results and discussion

After fabrication, we evaluated the imaging behaviors of these two PBLs. A collimated red light (635 nm) from a laser diode was applied to measure the focal length of PBL-1 and PBL-2. The measured results are both around 4 cm, as expected. To further investigate the performances in a smaller scale, a CMOS camera was used to measure the light intensity distribution along the optical axis near the focal points. Meanwhile, simulation results were also obtained using Zemax to compare with the experimental data.

Figure 3 shows the normalized intensity distribution at different planes along the optical axis, and the experimental data agree well with the simulation results. For PBL-1, when coming from the lens side to the focal point, the intensity at the outer circle is stronger than that of the central area as shown in Fig. 3(a). However, the intensity at the plane behind the focal point exhibits an opposite distribution, as Fig. 3(b) shows. The high-intensity area is in the center while the intensity at peripheral area gradually decreases. Theoretically, the two symmetric planes along the optical axis should have the same intensity distribution if the collimating lens is an ideal lens. However, due to the wavelength mismatch, the phase profile of PBL-1 deviates from that of an ideal lens, especially when the lens diameter gets larger. For PBL-2 fabricated using

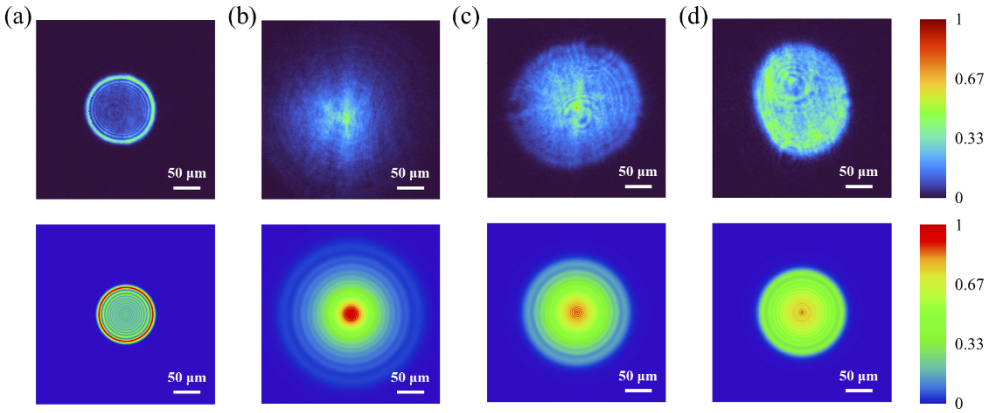

Fig. 3. Normalized experimental (top) and simulated (bottom) intensity distribution of PBLs at different positions: (a) 0.5 mm in front of PBL-1 focal point, (b) 0.5 mm behind PBL-1 focal point, (c) 0.5 mm in front of PBL-2 focal point, (d) 0.5 mm behind PBL-2 focal point.

Optics EXPRESS

the new method, the intensity of the two planes shows more similar distribution due to a much smaller deviation from the ideal lens phase profile. From Fig. 3, the maximum light intensity of our experimental results is lower than that of the simulated one. The main reason is due to the imperfect LC alignment caused by our two-layer spin-coating processes. In addition, some defects on each LC layer also degrade the PBL performance.

To investigate the imaging performance of our new lens, we built a Maxwellian display system as shown in Fig. 4(a) [21]. A laser projector was used as the light engine. The modulated output beam was then collimated by a lens, and a color filter was attached to the lens to avoid light leakage at other wavelengths. After passing through the PBLs, the light was focused to the pupil of a smartphone camera by PBLs, and the images were captured. The input image of vertical lines is depicted in Fig. 4(b), and the recorded images are shown in Fig. 4(c) for PBL-1 and Fig. 4(d) for PBL-2. The difference at the peripheral area is clearly observed. For Fig. 4(c), the vertical lines at the edges overlap with each other and only the lines at central area can be clearly observed. Some vertical lines in Fig. 4(c) and Fig. 4(d) are darker than other lines, which may result from the mismatched frame time between the laser projector and exposure time of the camera. In practical applications, the imaging performance may limit the field of view of the display system due to the degraded resolution caused by the phase deviation of PBL. The performance of PBL-2

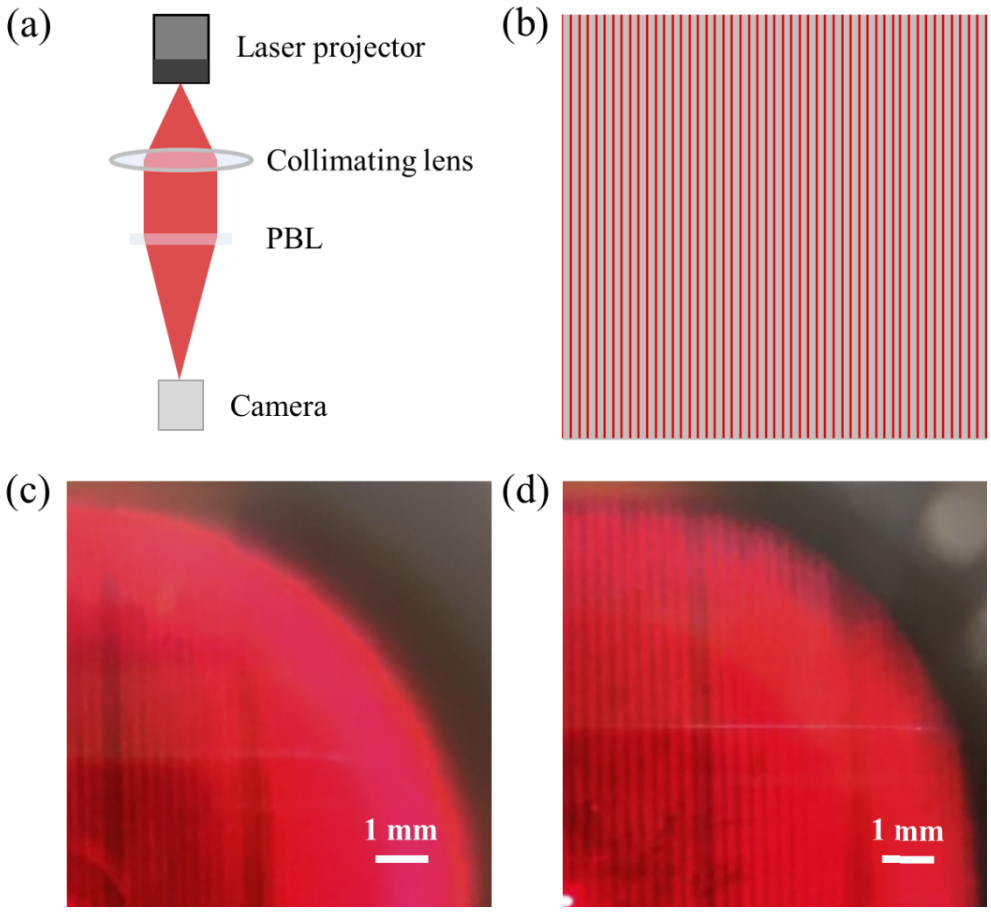

Fig. 4. (a) Maxwellian display system, (b) original input image, (c) recorded images with PBL-1, and (d) recorded images with PBL-2.

Optics EXPRESS

is much better since the vertical lines at the border can still be distinguished by the camera. The lines in some peripheral area of Fig. 4(d) cannot be separated, which may originate from the alignment problem during exposure process. Compared to previous exposure method, our new approach provides a much better image quality.

4. Conclusion

We demonstrated a new approach to correct the phase deviation of PBLs caused by the mismatched exposing and operating wavelengths. Using two lenses with different focal lengths in the exposure system, the newly designed PBL-2 exhibits a smaller phase difference from the ideal lens, which in turn leads to better imaging quality than the traditional PBL-1. The intensity of PBL-2 along optical axis shows more symmetric distribution about the focal point, which is like an ideal lens. The measured results agree well with the simulated intensity distribution. This new fabrication method is expected to make significant impact to AR/VR displays.

Funding. Goertek Electronics.

Disclosures. The authors declare no conflicts of interest.

Data availability. Data underlying the results presented in this paper are not publicly available at this time but may be obtained from the authors upon reasonable request.

References

1. S. Pancharatnam, "Generalized theory of interference and its applications," Proc. Indian Acad. Sci. **44**(6), 398–417 (1956).
2. M. V. Berry, "Quantal phase factors accompanying adiabatic changes," Proc. R. Soc. Lond. A **392**(1802), 45–57 (1984).
3. M. Attia and J. M. C. Jonathan, "Anisotropic gratings recorded from two circularly polarized coherent waves," Opt. Comm. **47**(2), 85–90 (1983).
4. L. Marrucci, C. Manzo, and D. Paparo, "Pancharatnam-Berry phase optical elements for wave front shaping in the visible domain: Switchable helical mode generation," Appl. Phys. Lett. **88**(22), 221102 (2006).
5. Y. Liu, Y. Ke, J. Zhou, Y. Liu, H. Luo, S. Wen, and D. Fan, "Generation of perfect vortex and vector beams based on Pancharatnam-Berry phase elements," Sci. Rep. **7**(1), 44096 (2017).
6. N. V. Tabiryan, D. E. Roberts, Z. Liao, J. Y. Hwang, M. Moran, O. Ouskova, A. Pshenichnyi, J. Sigley, A. Tabirian, R. Vergara, and L. De Sio, "Advances in transparent planar optics: enabling large aperture, ultrathin lenses," Adv. Opt. Mater. **9**(5), 2001692 (2021).
7. S. Liu, S. Qi, Y. Li, B. Wei, P. Li, and J. Zhao, "Controllable oscillated spin Hall effect of Bessel beam realized by liquid crystal Pancharatnam-Berry phase elements," Light: Sci. Appl. **11**(1), 219 (2022).
8. T. Zhan, Y. H. Lee, G. Tan, J. Xiong, K. Yin, F. Gou, J. Zou, N. Zhang, D. Zhao, J. Yang, S. Liu, and S. T. Wu, "Pancharatnam–Berry optical elements for head-up and near-eye displays," J. Opt. Soc. Am. B **36**(5), D52–D65 (2019).
9. J. Xiong and S. T. Wu, "Planar liquid crystal polarization optics for augmented reality and virtual reality: from fundamentals to applications," eLight **1**(1), 3 (2021).
10. J. Xiong, E. L. Hsiang, Z. He, T. Zhan, and S. T. Wu, "Augmented reality and virtual reality displays: emerging technologies and future perspectives," Light: Sci. Appl. **10**(1), 216 (2021).
11. K. Yin, E. L. Hsiang, J. Zou, Y. Li, Z. Yang, Q. Yang, P. C. Lai, C. L. Lin, and S. T. Wu, "Advanced liquid crystal devices for augmented reality and virtual reality displays: principles and applications," Light: Sci. Appl. **11**(1), 161 (2022).
12. T. Zhan, J. Xiong, Y. H. Lee, and S. T. Wu, "Polarization-independent Pancharatnam-Berry phase lens system," Opt. Express **26**(26), 35026–35033 (2018).
13. M. Fratz, S. Sinzinger, and D. Giel, "Design and fabrication of polarization-holographic elements for laser beam shaping," Appl. Opt. **48**(14), 2669–2677 (2009).
14. S. C. McEldowney, D. M. Shemo, R. A. Chipman, and P. K. Smith, "Creating vortex retarders using photoaligned liquid crystal polymers," Opt. Lett. **33**(2), 134–136 (2008).
15. L. De Sio, D. E. Roberts, Z. Liao, J. Hwang, N. Tabiryan, D. M. Steeves, and B. R. Kimball, "Beam shaping diffractive wave plates," Appl. Opt. **57**(1), A118–A121 (2018).
16. O. Yaroshchuk and Y. Reznikov, "Photoalignment of liquid crystals: basics and current trends," J. Mater. Chem. **22**(2), 286–300 (2012).
17. M. Schadt, K. Schmitt, V. Kozinkov, and V. Chigrinov, "Surface-induced parallel alignment of liquid crystals by linearly polymerized photopolymers," Jpn. J. Appl. Phys. **31**(7), 2155–2164 (1992).
18. O. Yaroshchuk, H. Gurumurthy, V. G. Chigrinov, H. S. Kwok, H. Hasebe, and H. Takatsu, "Photoalignment properties of brilliant yellow dye," Proc. International Display Workshops **7**, 1665–1668 (2007).

Optics EXPRESS

19. T. Yang, Y. Wang, D. Ni, D. Cheng, and Y. Wang, "Design of off-axis reflective imaging systems based on freeform holographic elements," Opt. Express **30**(11), 20117–20134 (2022).
20. Y. H. Lee, K. Yin, and S. T. Wu, "Reflective polarization volume gratings for high efficiency waveguide-coupling augmented reality displays," Opt. Express **25**(22), 27008–27014 (2017).
21. G. Westheimer, "The Maxwellian view," Vision Research **6**(11-12), 669–682 (1966).